


Chiral Stoner magnetism in Dirac bands

Zhiyu Dong¹* and Leonid Levitov¹*Department of Physics, Massachusetts Institute of Technology, Cambridge, Massachusetts 02139, USA* (Received 27 July 2022; revised 15 May 2024; accepted 23 May 2024; published 13 September 2024)

Stoner magnetism in bands endowed with Berry curvature is shown to be influenced by the coupling between spin-chirality density $\mathbf{s} \cdot (\partial_x \mathbf{s} \times \partial_y \mathbf{s})$ and Berry's orbital magnetization. The key effect is that carriers moving in the presence of a spin texture see it as a source of a geometric magnetic field coupled to the carrier's orbital motion through a spin-dependent Aharonov-Bohm effect. This interaction was recently predicted to enable chiral magnons propagating along system boundaries. Here we show that it also favors chiral spin textures such as skyrmions—the topologically protected objects with particle-like properties, stabilized in the ground state. Unlike previously studied systems, here skyrmion textures can arise in the absence of microscopic spin-dependent interactions such as spin-orbit coupling or Zeeman coupling. The threshold for Stoner instability is found to soften, rendering chiral spin-ordered phases accessible under realistic conditions. We present a detailed analysis of the chiral effect for Bernal bilayer graphene and discuss the unique properties of skyrmion textures in graphene multilayers.

DOI: [10.1103/PhysRevB.110.104420](https://doi.org/10.1103/PhysRevB.110.104420)

The advent of electron systems hosting topological flat bands and strong interactions [1–5] raises fascinating questions about the impact of Berry curvature on many-body physics. Recent work has focused on graphene multilayers such as moiré graphene [6–12], where flat bands emerge when the moiré twist angle is tuned to a magic value [4]. Additionally, research has explored field-biased non-moiré bilayers and trilayers [13–17], systems in which bands are flattened by a transverse electric field [18]. The small kinetic energy of carriers in flattened bands and the strong electron interactions characteristic of graphene create a setting in which a variety of ordered many-body phases can be realized and explored. The wide variety of observed orders, including cascades of magnetic phases polarized in isospin (spin and valley) alongside the insulating and superconducting phases, prompts seeking new interactions and previously unknown many-body orders in these systems.

With this motivation, here we consider itinerant magnetic metals with spontaneously spin-polarized carriers in bands equipped with Berry curvature. We find that such systems possess a geometric coupling of the orbital and spin degrees of freedom that favors nonzero spin chirality $\mathbf{s} \cdot (\partial_1 \mathbf{s} \times \partial_2 \mathbf{s})$, where $\mathbf{s}(x)$ is the spin density and $\partial_{1,2}$ are spatial derivatives. Such geometric coupling, enabled by Berry curvature and electron exchange interactions, is allowed to exist by general symmetry arguments. Below we develop a microscopic theory of this effect, with a particular focus on itinerant graphene flat-band systems in which carriers are polarized in spin and/or valley (the 1/2-metal and 1/4-metal phases) as well as partially isospin-polarized (PIP) phases. The underlying physics can be understood as electromagnetic coupling $-\mathbf{M}\mathbf{B}$ between orbital magnetization \mathbf{M} due to the band Berry curvature and

the geometric magnetic field \mathbf{B} originating from spin chirality. From a more general point of view, it can be thought of as an emergent spin-orbit interaction (SOI) driven by electron exchange, with the coupling strength taking a universal value mandated by properties of the geometric phase and topological constraints.

This geometric SOI has several implications. One is the existence of new collective excitations—chiral magnons propagating along the edges of the system [19]. These chiral spin waves, induced by the geometric SOI, are expected to emerge robustly in all itinerant spin-polarized phases in bands with Berry curvature. Another implication, discussed in this paper, is the emergence of new magnetic phases in which spins form textures such as spin-density waves or skyrmions. Below, after demonstrating the effect microscopically, we analyze the stability of a uniformly polarized phase. We find that in the presence of geometric SOI, it becomes unstable towards formation of skyrmion textures at sufficiently low carrier densities (see Fig. 1).

The interplay between orbital effects and spin degrees of freedom is a topic that has been widely studied in magnetism, where microscopic spin-orbit interactions have been used to stabilize different kinds of helical and chiral orders in magnetic systems. Of special interest are the chiral magnetic phases, wherein spins wrap around the Bloch sphere. Chiral spin textures have been explored in various magnetic systems [20,21]. In systems explored to date, chirality is typically driven by spin-orbit interactions, such as the Dzyaloshinskii-Moriya (DM) coupling. This interaction favors a variety of spin textures [22], including helical spin-density waves [23–25] and skyrmions—the seminal topologically protected particle-like spin configurations [26]. Much less is known about the possibility to achieve a chiral spin order in graphene-based systems. At first sight, this may seem problematic as staple SOI interactions that stabilize chiral magnetic orders are absent or extremely weak in graphene. Indeed, in

*Present address: Physics Department, California Institute of Technology.

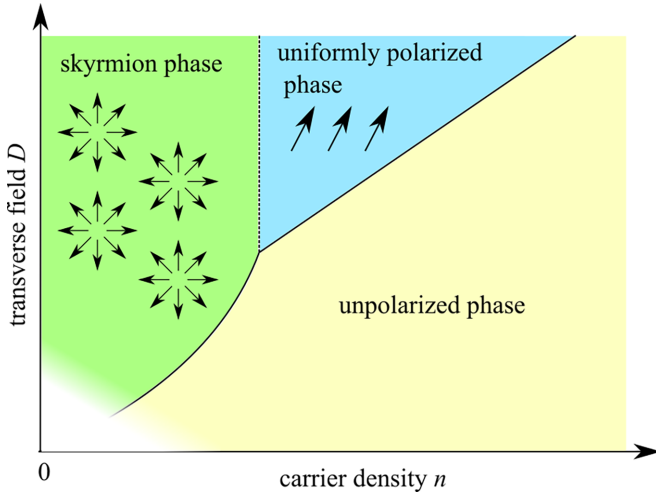


FIG. 1. The mean-field phase diagram for chiral magnetic order in the quadratic Dirac model, Eqs. (4) and (6), away from charge neutrality at $D = 0$. Transition between uniformly spin-polarized and unpolarized phases is first-order, occurring on a straight line in the n - D plane given by Eq. (42). Transition between skyrmion phase and uniformly polarized phase is second order, with skyrmion density vanishing at the phase boundary given by Eq. (53). Phase boundaries are found by focusing on spin polarization in one valley and ignoring valley ordering (see text).

noncentrosymmetric magnets—the bulk chiral magnetic metals [27–32] and magnetic layers [33,34]—skyrmions are stabilized by the DM coupling governed by the microscopic spin-orbit interactions [20,22]. However, the microscopic SOI in graphene is usually negligible compared to other energy scales [35]. Likewise, the mechanisms that utilize frustration [36–38] are not found in graphene systems. Yet, as will be demonstrated below, the geometric SOI originating from the interplay of a band curvature and spin polarization can mimic some of the physics emerging from the conventional SOI. In particular, it favors chiral spin orders without requiring interactions breaking $SU(2)$ spin-rotation symmetry, microscopic SOI or frustrations. These effects provide an alternative route to phases with helical and chiral spin order. The geometric SOI effect therefore provides an appealing route to phases with chiral spin order, such as skyrmion crystals and liquids.

I. SYMMETRY OF THE CHIRAL EFFECT

The quantity that will be central to our discussion is the chirality density, or topological density, of a spin texture $\mathbf{s}(\mathbf{x})$ defined as a scalar triple product

$$\Omega(\mathbf{x}) = \frac{1}{2} \epsilon_{\mu\nu} \mathbf{s}(\mathbf{x}) \cdot (\partial_\mu \mathbf{s}(\mathbf{x}) \times \partial_\nu \mathbf{s}(\mathbf{x})), \quad (1)$$

where $\epsilon_{\mu\nu}$ a 2×2 antisymmetric tensor. This quantity, which characterizes spin density twisting in the texture, has several properties mandated by symmetry. First, despite being a function of angles, which cannot be reduced to a function of the modulus $|\mathbf{s}|$, chirality is invariant under $SU(2)$ spin rotations. Second, it is odd under time-reversal and spin-reversal operations, $t \rightarrow -t$ and $\mathbf{s} \rightarrow -\mathbf{s}$. The $SU(2)$ symmetry property suggests that chirality could emerge from the standard spin-

exchange interaction that obeys $SU(2)$ symmetry. However, being odd under time- and spin-reversal symmetries excludes this quantity from basic models of magnetism such as the Heisenberg model and its extensions. Yet, as we will see, this quantity is required by symmetry for magnetism in bands with Berry curvature.

Specifically, despite its exotic symmetry properties, this quantity appears naturally in the problem of itinerant spin magnetism in Dirac bands such as those found in graphene multilayers, moiré [4,6,39] and non-moiré [18,40]. In these systems carriers reside in valleys K and K' that are mapped to one another under time-reversal symmetry. At the same time, the band dispersion and interactions in each valley individually are not constrained by time- and spin-reversal symmetries. As a result, the symmetry constraints for the quantities such as chirality are relaxed. Allowed by the symmetries of the microscopic Hamiltonian, these quantities must be included in the theoretical description of the magnetic order. Furthermore, the analysis described below, which links these quantities to geometric gauge fields, predicts a universal value of the coupling constant that is large enough to significantly alter the physics of the ordered phase. As we will see, the interaction proportional to the chirality density in Eq. (1) can lower the threshold for Stoner instability and stabilize chiral spin textures in the ordered phase. Figure 1 illustrates this for a quadratic Dirac band model of field-biased bilayer graphene (BBG) analyzed below.

The effect responsible for this behavior arises from the coupling between orbital magnetization due to k -space Berry curvature of Dirac carriers and chirality density of position-dependent spin polarization, described as

$$\delta F = \int d^2x \sum_{i=K,K'} -(M_{i,+} - M_{i,-}) b_i(\mathbf{x}), \quad (2)$$

where $M_{i,\pm}$ is the orbital magnetization of the majority-spin and minority-spin carriers in valleys K and K' [see Eq. (35)]. This interaction can be viewed as an extension of the basic electromagnetic coupling of a magnetic moment and external field, $E = -\mathbf{M} \cdot \mathbf{B}$, where the “magnetic field” $b_i(\mathbf{x})$ is defined as topological density of spin texture in each valley multiplied by the flux quantum ϕ_0 ,

$$b_i(\mathbf{x}) = \frac{\phi_0}{4\pi} \mathbf{s}_i \cdot (\partial_1 \mathbf{s}_i \times \partial_2 \mathbf{s}_i), \quad \phi_0 = hc/e, \quad (3)$$

with $\mathbf{s}_i(\mathbf{x})$ the unit-vector field representing spin polarization of carriers in valleys $i = K, K'$. The quantity $b_i(\mathbf{x})$ represents a geometric “magnetic field” associated with the spin-dependent (geometric or chiral) Aharonov-Bohm effect. This effect originates from the fundamental properties of spin textures $\mathbf{s}_i(\mathbf{x})$ in which the position-dependent quantization axis along which carrier spins are polarized is, in general, allowed to twist in space. Spins of carriers moving through a texture and coupled to it by exchange undergo adiabatic spin rotation, which leads to geometric phase and magnetic field $b_i(\mathbf{x})$ associated with the Aharonov-Bohm effect due to this phase. The magnetic field originates from carrier movement through the texture, is coupled to orbital degrees of freedom of carriers, leading to the $-\Delta M_i b_i$ coupling to orbital magnetization of carriers appearing in Eq. (2).

Since M_i describes orbital magnetization whereas b_i is a property of spin degrees of freedom, the interaction in Eq. (2) can be viewed as an emergent spin-orbit coupling effect that originates from spin exchange and does not rely on a microscopic spin-orbital coupling. To understand the symmetry properties of this interaction, it is instructive to compare it to the atomic spin-orbital interaction (SOI) $E \sim \mathbf{L} \cdot \mathbf{S}$. The SOI locks spin polarization s to the orbital angular momentum vector \mathbf{L} . As a result, it is not invariant under SU(2) spin rotations. To the contrary, the chiral interaction originates from microscopic SU(2)-invariant spin exchange interactions, and is therefore invariant under spin rotations. Indeed, both quantities featured in Eq. (2)—the direct-space geometric phase, which gives rise to $b_i(\mathbf{x})$, and momentum-space Berry curvature responsible for $M_{i,\pm}$ are SU(2)-invariant. As a result, perhaps somewhat unexpectedly, the chiral interaction in Eq. (2) is also invariant under spin rotations. This is a high symmetry which is not expected for interactions originating from a microscopic SOI but is completely natural for geometric SOI considered here.

Furthermore, the interaction in Eq. (2) also respects discrete symmetries of BBG, including the time-reversal and mirror symmetries. Indeed, the time-reversal symmetry maps s_K to $-s_{K'}$, therefore it maps b_K to $-b_{K'}$. Simultaneously, the orbital magnetization M_K is mapped to $-M_{K'}$. Consequently, Eq. (2) is invariant under time-reversal symmetry. Likewise, the mirror symmetry maps M_K to $-M_{K'}$, whereas b_K is mapped to $-b_{K'}$. Indeed, taking for example the mirror lying in yz plane, the gradient components (∂_1, ∂_2) are mapped to $(-\partial_1, \partial_2)$, leaving the chirality density in Eq. (1) unchanged. Consequently, Eq. (2) respects mirror symmetry. Same conclusion applies to the other two mirrors as they are equivalent to the yz mirror up to a C_3 rotation.

We note that in this reasoning, due to the absence of microscopic SOI, the spin and orbital degrees of freedom are decoupled and we do not need to account for the mirror symmetry action on spin degrees of freedom. However, it is straightforward to show that the conclusion would remain the same if we accounted for mirror symmetry action on spin. Indeed, the yz mirror maps $s_K = (s_K^x, s_K^y, s_K^z)$ to $(s_{K'}^x, -s_{K'}^y, -s_{K'}^z)$, which leaves the chiral density invariant. Further, we note parenthetically that the C_2 symmetry that interchanges the top and bottom graphene layers is broken in the systems of interest due to the presence of a transverse electric field. This is a crucial condition for the system to host the chiral coupling because otherwise (in the presence of the C_2 symmetry) the orbital magnetization would not be allowed by symmetry and must vanish.

This discussion demonstrates that the interaction given in Eq. (2) follows the form allowed by symmetry. This symmetry property has two implications. First, while the interaction in Eq. (2) obeys the continuous spin-rotation symmetry as well as the discrete time-reversal and mirror symmetries, these symmetries may be broken in the system ground state, either together or individually, leading to a variety of broken-symmetry phases. Indeed, as illustrated by Fig. 1, this is what happens in the system of interest. Second, all interactions of the form allowed by symmetry are expected to be supported by a generic realistic Hamiltonian. Therefore, the details of the microscopic derivation presented below notwithstanding,

all conclusions of our analysis can be justified based on symmetry grounds alone. This makes the results of the analysis presented below applicable broadly, being valid outside the specific assumptions under which the analysis will be carried out. Likewise, from the symmetry point of view, the properties of electron bands in rhombohedral multilayer graphene are the same as those in BBG. Therefore, the analysis carried out for BBG is applicable to a wider variety of multilayer graphene systems, such as rhombohedral-stacked trilayer, tetralayer and pentalayer graphene.

It is also worth noting that the chiral interaction that stabilizes skyrmions in our theory is distinct from various effects considered in the literature. In particular, skyrmions in isospin-polarized moiré graphene flat bands have been invoked to predict exotic superconductivity [41,42]. The mechanism that stabilizes skyrmions in these papers is an isospin extension of quantum Hall ferromagnet physics, in which skyrmions emerge in Landau levels spin-split by exchange interactions [21,43–45]. Skyrmions of this type have been predicted [46,47] and recently observed [48,49] in graphene at high magnetic fields.

II. ITINERANT MAGNETISM IN A BAND WITH BERRY CURVATURE

Here, we discuss Stoner magnetism in a graphene bilayer Dirac band. This analysis will set the stage for deriving microscopically the interaction between spin-chirality and orbital magnetization enabled by Berry curvature, Eq. (2). This will be achieved by perturbation theory expansion in gradients of spatially varying spin polarization, assumed to be weak. Our starting point is a fully SU(2)-invariant Hamiltonian involving a single-particle Hamiltonian and electron-electron interactions, but not involving any microscopic SOI,

$$\mathcal{H} = \mathcal{H}_0 + \mathcal{H}_{\text{int}}. \quad (4)$$

We take the single-particle part \mathcal{H}_0 to be a quadratic Dirac Hamiltonian of a Bernal-stacked graphene bilayer

$$\mathcal{H}_0 = \sum_{\eta,p} c_{\eta,p}^\dagger H_\eta(p) c_{\eta,p} \quad (5)$$

where $H_\eta(p)$ is a 2×2 Hamiltonian

$$H_\eta(p) = \begin{pmatrix} D & \frac{(p_1 - i\eta p_2)^2}{2m} \\ \frac{(p_1 + i\eta p_2)^2}{2m} & -D \end{pmatrix}. \quad (6)$$

Here, $\eta = \pm 1$ for the valleys K and K' ; the quantities $c_{\eta,p}$, $c_{\eta,p}^\dagger$ are spinors with the A and B sublattice components and the ordinary spin-1/2 components. The Hamiltonian $H_\eta(p)$ possesses particle-hole symmetry, with the effects of particle-hole asymmetry and trigonal warping ignored for simplicity. Incorporating these terms later or generalizing to other Dirac band types would be straightforward. Estimates for realistic parameter values are provided in Sec. VII [see discussion beneath Eq. (53)].

Next, we consider the electron-electron interaction. For simplicity, we focus on the intravalley spin exchange and ignore the exchange interaction between electrons in valleys K and K' . The inter-valley processes are expected to be weak as they involve a large momentum transfer, and are therefore subleading to the intra-valley processes. Indeed,

the electron-electron interaction predominantly arises from Coulomb interaction, which decreases as $1/k$ as a function of the momentum transfer k . Restricting the exchange interaction to electrons in the same valley, we introduce a spin-exchange coupling of the form

$$\mathcal{H}_{\text{int}} = -\frac{1}{2} \sum_{\eta, \mathbf{k}} U(\mathbf{k}) : s_{\eta\alpha}(\mathbf{k}) s_{\eta\alpha}(-\mathbf{k}) : . \quad (7)$$

Here the exchange interaction is written in terms of spin density $s_{\eta\alpha}(\mathbf{k}) = \sum_p c_{\eta, p+k}^\dagger \sigma_\alpha c_{\eta, p}$ with Pauli matrices σ_α representing ordinary spin-1/2 variables, $\alpha = 1, 2, 3$. Microscopically, the spin-exchange coupling originates from the Coulomb interaction. However, directly starting from microscopic interactions will significantly complicate the analysis. Here, to illustrate the physics of interest within a simplest formulation, we replace the microscopic exchange interaction with a toy-model dependence

$$U(\mathbf{k}) = U_0 e^{-k^2 \xi^2}, \quad (8)$$

where ξ is a correlation lengthscale.

Equivalently, the spin-exchange Hamiltonian given in Eq. (7) can be written in coordinate representation as

$$\mathcal{H}_{\text{int}} = \sum_{\eta} -\frac{1}{2} \sum_{\mathbf{x}, \mathbf{x}'} U(\mathbf{x} - \mathbf{x}') : s_{\eta\alpha}(\mathbf{x}) s_{\eta\alpha}(\mathbf{x}') : , \quad (9)$$

with a nonlocal spin-spin interaction

$$U(\mathbf{x} - \mathbf{x}') = 4\pi U_0 \xi^{-2} e^{-(\mathbf{x} - \mathbf{x}')^2 / 4\xi^2} \quad (10)$$

normalized to $\int d^2x U(\mathbf{x}) = U_0$. As we will see, tuning the interaction radius ξ provides a convenient knob for studying the spin-polarized phase, analyzing fluctuations and charting the phase diagram of skyrmion textures.

In our model, given by Eqs. (6) and (7), the electrons in two valleys are decoupled. Therefore, in the analysis below we can consider the K valley alone. It should be noted that in reality the electrons in valleys K and K' also interact through a direct density-density interaction (the Hartree energy). However, we do not need to include this interaction in the model because this term only gives a charging energy that determines the total electron density. As such, it does not affect the spin polarization in each valley, which is quantity of interest.

III. MEAN-FIELD THEORY FOR SPIN TEXTURES

To describe spin textures, we perform a mean-field analysis in which the field describing ensemble-averaged spin polarization is allowed to vary in space. Since the exchange interactions are predominantly intravalley it will be sufficient to carry out the analysis for an individual valley and consider the role of valley degrees of freedom later. The Hubbard-Stratonovich (HS) transformation is carried out using an ordering field $\mathbf{h}(\mathbf{x})$ with both the modulus and orientation

being position-dependent,

$$\begin{aligned} & \exp \left(\int dt \sum_{\mathbf{k}} \frac{U(\mathbf{k})}{2} s_{\mathbf{k}} \cdot s_{-\mathbf{k}} \right) \\ &= \int D[\mathbf{h}] \exp \left(\int dt \sum_{\mathbf{k}} \mathbf{h}_{\mathbf{k}}(t) \cdot s_{-\mathbf{k}} - \frac{\mathbf{h}_{\mathbf{k}}(t) \mathbf{h}_{-\mathbf{k}}(t)}{2U(\mathbf{k})} \right), \end{aligned} \quad (11)$$

where $D[\mathbf{h}] = \prod_{\mathbf{k}, t} d\mathbf{h}_{\mathbf{k}}(t)$. Here we introduced Fourier harmonics of the HS field and spin density $\mathbf{h}_{\mathbf{k}} = \int d^2x \mathbf{h}(\mathbf{x}) e^{-i\mathbf{k}\mathbf{x}}$, $s_{\mathbf{k}} = \int d^2x s(\mathbf{x}) e^{-i\mathbf{k}\mathbf{x}}$. Integrating out fermions and assuming a time-independent $\mathbf{h}(\mathbf{x})$, we obtain the free energy with a nonlocal $h(\mathbf{x})h(\mathbf{x}')$ interaction

$$F = \text{Tr} \log [i\omega - H(p) - h_\alpha(\mathbf{x})\sigma_\alpha] + \sum_{\mathbf{k}} \frac{\mathbf{h}_{\mathbf{k}} \mathbf{h}_{-\mathbf{k}}}{2U(\mathbf{k})}, \quad (12)$$

where, for conciseness, the chemical potential μ is incorporated in H and Tr denotes $\sum_{\mathbf{x}} \int \frac{d\omega d^2p}{(2\pi)^3} \text{Tr}_{2 \times 2}$. Equation (12) is an exact result for the fermion partition function, with no approximations made, which is applicable for any position-dependent ordering field $\mathbf{h}(\mathbf{x})$.

In this framework, the behavior of the states with uniform polarization and those with a general space- and time-dependent $\mathbf{h}(\mathbf{x}, t)$ can be compared on equal footing. The saddle point condition $\delta F = 0$ yields a time-independent $h = |\mathbf{h}|$, which is nothing but the Stoner mean-field value

$$h = U(0)(n_+ - n_-)/2, \quad (13)$$

where n_+ and n_- are local densities of carriers with spins parallel and antiparallel to local spin quantization axis $\mathbf{h}(\mathbf{x})$. We will call these spin species the majority and the minority spins, respectively. When the system is fully polarized, the mean field equals $h = U(0)n/2$.

Next, we consider weakly inhomogeneous $\mathbf{h}(\mathbf{x})$. The term $-h_\alpha(\mathbf{x})\sigma_\alpha$ describes electron spins coupled to a spin texture with a position-dependent magnetization polarized along the unit vector $\mathbf{s}(\mathbf{x}) = \mathbf{h}(\mathbf{x})/h$, where $|\mathbf{h}(\mathbf{x})| = h$. We therefore write $\mathbf{h}(\mathbf{x}) = \mathbf{h}_0 + \delta\mathbf{h}(\mathbf{x})$, where $\delta\mathbf{h}(\mathbf{x}) \perp \mathbf{h}_0$, and approximate the dependence of the free energy on $\delta\mathbf{h}(\mathbf{x})$ as a second-order functional derivative

$$\delta F = F[\mathbf{h}(\mathbf{x})] - F[h_0] = \sum_{\mathbf{k}} \frac{1}{2} \frac{\partial^2 F}{\partial \mathbf{h}_{\mathbf{k}} \partial \mathbf{h}_{-\mathbf{k}}} \delta \mathbf{h}_{\mathbf{k}} \delta \mathbf{h}_{-\mathbf{k}}, \quad (14)$$

where $F[h_0]$ is the free energy evaluated for spatially uniform $\mathbf{h}(\mathbf{x})$. Expanding the logarithmic term in the free energy [Eq. (12)] in $\delta\mathbf{h}(\mathbf{x})$ to second order yields

$$\delta F = \sum_{\mathbf{k}} \frac{1}{2} \chi_{\pm}(\mathbf{k}) \delta \mathbf{h}_{\mathbf{k}} \cdot \delta \mathbf{h}_{-\mathbf{k}} + \frac{\delta \mathbf{h}_{\mathbf{k}} \cdot \delta \mathbf{h}_{-\mathbf{k}}}{2U(\mathbf{k})}, \quad (15)$$

where $\chi_{\pm}(k)$ is the Lindhard function of spin-polarized Fermi sea.

This result can be used to evaluate spin stiffness. In doing so, we expect that the $\mathbf{k} = 0$ contributions of $\chi_{\pm}(k)$ and $1/U(k)$ cancel out, since only the spatially varying part of $\mathbf{h}(\mathbf{x})$ contributes to the energy of a weakly inhomogeneous symmetry-broken state (as required by Goldstone's theorem) [50]. Accordingly, we consider the dependence F vs. $\delta\mathbf{h}_{\mathbf{k}}$

assuming that the local spin-quantization axis is slowly varying, $\xi \partial_\mu S_\alpha \ll 1$. This is the case when large spin stiffness makes the short-wavelength fluctuations in $\mathbf{h}(\mathbf{x})$ costly and, therefore, weak. Expanding in k at second order, $U^{-1}(k) \approx U^{-1}(0)(1 + k^2 \xi^2)$, $\chi_\pm(k) \approx \chi_\pm(0) + ak^2$, gives the dependence of the free energy on $\delta \mathbf{h}_k$,

$$\delta F = \sum_k \frac{1}{2} \left(\chi_\pm(0) + ak^2 + \frac{1 + k^2 \xi^2}{U(0)} \right) \delta \mathbf{h}_{-k} \delta \mathbf{h}_k. \quad (16)$$

Taking into account that $\chi_\pm(k)$ is evaluated for the spin-polarized state, we confirm that $k = 0$ contributions cancel out owing to the Stoner mean-field relation, Eq. (13). This yields the gradient expansion

$$\delta F = \sum_x \frac{1}{2} J (\partial_\mu S_\alpha)^2, \quad J = \frac{\xi^2 \hbar^2}{U(0)} + ah^2. \quad (17)$$

This result indicates that the spin-stiffness parameter J is dominated by $U(k)$ expansion to order k^2 when the correlation length ξ is large. For a contact interaction the stiffness is dominated by Lindhard function expansion. For a realistic short-range interaction, both contributions to stiffness are expected to be equally important.

The value and sign of a are sensitive to the details of the band structure and may potentially result in a negative spin stiffness J . To ensure that J remains positive, we focus here on the large- ξ regime where $\xi^2 \gg aU(0)$. In this case, the stiffness value is dominated by the first term in Eq. (17),

$$J \approx \frac{\xi^2 \hbar^2}{U(0)}. \quad (18)$$

The positivity of J is crucial because otherwise, a spin-density wave pattern would emerge, rendering the approach relying on perturbation theory around the uniform saddle point invalid.

IV. SPIN-DEPENDENT GEOMETRIC MAGNETIC FIELD

Next, we extend the mean-field framework to describe spin textures. This can be done by considering the spatial dependence of the spin-polarization field $\mathbf{h}(\mathbf{x})$. In this section, we show that the spin texture generates a geometric spin-dependent magnetic field $b(\mathbf{x})$ given by Eq. (3), which couples to electrons as described in Eq. (2).

We first give a heuristic argument for the origin of the field $b(\mathbf{x})$. Microscopically, it arises from the adiabatic spin-rotation effect for spins of electrons moving through a long-period spin texture to which they are coupled by exchange interaction. The spin rotation describes evolution of an electron spin being locked to the local spin-quantization axis and tracking it along the electron trajectory. In the adiabatic regime, the effect can be described by a spin-dependent geometric phase that depends on position-dependent spin polarization in the texture. This adiabatic framework is applicable when the Stoner spin gap is large compared to $\hbar v/\ell$, where ℓ is the characteristic spatial lengthscale of the spin-texture modulation and v is the Fermi velocity. Berry curvature associated with the vector potential describing this geometric phase, defines a geometric magnetic field

$$b(\mathbf{x}) = \frac{\hbar c}{e} \hat{z} \cdot [\nabla_{\mathbf{x}} \times \mathbf{a}(\mathbf{x})]. \quad (19)$$

Below, we derive the quantities \mathbf{a} and b from spin-dependent gauge fields obtained from the microscopic Hamiltonian. By carrying out an expansion in gradients of a , assumed to be small, we demonstrate that b equals, up to a universal factor, to the chirality density given in Eq. (1). From this, we derive the geometric coupling between b and electrons' orbital magnetization, which is the interaction given in Eq. (2).

Next, we formally introduce a gauge field describing a position-space Berry phase for electrons in the presence of a slowly varying spin texture. In that we follow the procedure developed some time ago in the literature on quantum antiferromagnets and high-temperature superconductivity [51–54] (see also [55]) and, more recently, in the literature on frustrated magnetic systems [56–58]. Below we present a step-by-step derivation of the gauge field picture starting with the microscopic Hamiltonian introduced in Sec. II. In doing so, it will be shown explicitly that a spin texture gives rise to an effective gauge field whose flux density is associated with the spin chirality. In our analysis below, without loss of generality, we focus on spins in valley K and suppress the valley label. A spin texture is described by a position-dependent ordering field $\mathbf{h}(r)$ introduced in Sec. III through a Hubbard-Stratonovich mean-field analysis, which we will write as

$$\mathbf{h}(\mathbf{x}) = h\mathbf{s}(\mathbf{x}) \quad (20)$$

where $\mathbf{s}(\mathbf{x})$ is a unit-vector field, $|\mathbf{s}(\mathbf{x})| = 1$. In what follows, we will ignore fluctuations of the order parameter magnitude h and focus on the fluctuations of $\mathbf{s}(\mathbf{x})$ orientation in spin space.

The first step is to perform an SU(2) spin rotation to bring all the local spin polarization to the same orientation and, in this way, generate a Hamiltonian that features a geometric spin-dependent gauge field. We start with a one-electron Hamiltonian in valley K , writing it in position space,

$$H(r) = \left(\begin{array}{cc} D & \frac{(p_1 - ip_2)^2}{2m} \\ \frac{(p_1 + ip_2)^2}{2m} & -D \end{array} \right) 1_S - h 1_L \mathbf{s}(r) \cdot \boldsymbol{\sigma} \quad (21)$$

where 1_S and 1_L represent the identity matrices in the spin and sublattice subspaces, respectively. In the first term, $p_{1,2} = -i\partial_{1,2}$ (here we set $\hbar = 1$, restoring dimensional units later). The second term represents the effect of a position-dependent spin polarization arising after a Hubbard-Stratonovich transformation, see Eq. (12).

The coordinate-dependent spin-rotation operator $T(\mathbf{x})$ that rotates all spins from the local polarization direction $\mathbf{s}(\mathbf{x})$ to the $+z$ direction is defined through

$$|z\pm\rangle = T(\mathbf{x}) |\mathbf{s}(\mathbf{x})\pm\rangle. \quad (22)$$

When acting with this spin rotation on the Hamiltonian in Eq. (21), the coordinate-dependent ordering field in the term $\mathbf{h}_\alpha(\mathbf{x})\sigma_\alpha$ is transformed to a uniform field pointing in $+z$ direction,

$$h\sigma_3 = T(\mathbf{x}) \mathbf{h}_\alpha(\mathbf{x}) \sigma_\alpha T^\dagger(\mathbf{x}). \quad (23)$$

However, the simplicity comes at a price: the momentum operator in the Hamiltonian, Eq. (21), is transformed by T to a long derivative with a 2×2 matrix gauge field. Namely,

the Hamiltonian is transformed to

$$H_z(\mathbf{x}) = T(\mathbf{x})H(\mathbf{x})T^\dagger(\mathbf{x}),$$

$$= \begin{pmatrix} D & \frac{(\Pi_1 - i\Pi_2)^2}{2m} \\ \frac{(\Pi_1 + i\Pi_2)^2}{2m} & -D \end{pmatrix} 1_S - \hbar 1_L \sigma_3 \quad (24)$$

where

$$\Pi_\mu = -iT(\mathbf{x})\partial_\mu T^\dagger(\mathbf{x}) = p_\mu + A_\mu,$$

$$A_\mu = -iT(\mathbf{x})[\partial_\mu, T^\dagger(\mathbf{x})], \quad \mu = 1, 2. \quad (25)$$

Here $A_{1,2}$ are 2×2 matrices representing an SU(2) gauge field, and the square brackets represent commutators. The quantities A_μ can be expressed in terms of Pauli matrices,

$$A_\mu = \sum_{i=1,2,3} a_{\mu,i} \sigma_i, \quad (26)$$

where the coefficients $a_{\mu,i}$ are the scalar quantities

$$a_{\mu,i}(\mathbf{x}) = \frac{1}{2} \text{Tr}(\sigma_i A_\mu) = -\frac{i}{2} \text{Tr}(\sigma_i T(\mathbf{x})\partial_\mu T^\dagger(\mathbf{x})). \quad (27)$$

This analysis, which is exact so far, simplifies in the adiabatic regime, where all spins track the spin-up and spin-down states in rotated basis. In this case, the off-diagonal components $a_{\mu,1}$ and $a_{\mu,2}$ describe coupling between spin states split by exchange. Such couplings only contribute at subleading order since they induce off-resonant transitions between local spin-up and spin-down states, which are weak in the adiabatic limit. We can therefore retain only the diagonal σ_3 spin components, given by Eq. (27). This gives

$$\Pi_\mu = p_\mu + a_\mu \sigma_3, \quad (28)$$

where from now on a_μ will be used as a shorthand for $a_{\mu,3}$. Plugging this back to Eq. (24), and absorbing μ in $H_z(p)$, we have the following form of free energy

$$F = \text{Tr} \log [i\omega - H_z(\mathbf{p} + \mathbf{a}\sigma_3) - \hbar\sigma_3] + F_h \quad (29)$$

where Tr denotes $\int d^2x \sum_{\omega,p} \text{Tr}_{2 \times 2}$ and F_h is the spin-stiffness energy given in Eq. (16).

The results indicate that the spin-up and spin-down electrons in the rotated basis, describing the majority and minority spin in the original basis, experience $U(1)$ gauge fields of opposite signs. After some algebra, which follows closely that in Ref. [57], one finds

$$a_\mu = -\frac{1}{2}(1 - \cos \theta)\partial_\mu \phi \quad (30)$$

where θ and ϕ are the spherical polar and azimuthal angles measured with respect to the z axis introduced in Eq. (22). The geometric magnetic field $b = \frac{\hbar c}{e} \hat{z} \cdot [\nabla \times \mathbf{a}]$ is then given by

$$b(\mathbf{x}) = \frac{\hbar c}{e} \epsilon_{\mu\nu} \partial_\nu a_\mu = \frac{\hbar c}{2e} \epsilon_{\mu\nu} \mathbf{s} \cdot (\partial_\mu \mathbf{s} \times \partial_\nu \mathbf{s}), \quad (31)$$

which is nothing but the chirality density given in Eq. (1). The result in Eq. (30) indicates that the geometric phase picked up by an electron moving in the magnetic field $b(\mathbf{x})$ is equal to $1/2$ of the solid angle swept by the spin-quantization axis.

So far, we have utilized the ‘‘geometric’’ units where $\hbar = 1$ and the units for \mathbf{p} and \mathbf{a} are inverse length. Consequently, the geometric field b is expressed in units of inverse length squared. It is interesting to examine how these quantities and their relationships alter when physical units are restored, setting the units for p_μ and a_μ to \hbar over length.

The relationship between Π_μ and p_μ given in Eq. (28) remains unchanged upon reintroducing physical \hbar units. It is instructive to compare Eq. (28) to the canonical electromagnetic coupling,

$$\mathbf{\Pi} = \mathbf{p} - \frac{e}{\hbar c} \mathbf{A}. \quad (32)$$

Clearly, while the coupling between the geometric field \mathbf{a} and orbital degrees of freedom in Eq. (28) mirrors the canonical coupling in form, the coupling strength is quite different from that in Eq. (32). This has a number of implications. Notably, the coupling to geometric gauge field leads to energy scales that are independent of e and c . Therefore, these energy scales are not small in the electromagnetic fine structure parameter $1/137$. Rather, the energy scales are governed by the length-scales describing spatial periodicity of skyrmion textures and can be relatively large [see Eq. (56) and accompanying discussion].

V. GRADIENT EXPANSION IN $\mathbf{a}(\mathbf{x})$

The analysis in Sec. IV establishes that the geometric magnetic field $b = \frac{\hbar c}{e} \hat{z} \cdot [\nabla \times \mathbf{a}]$ is perceived by electrons as a pseudomagnetic field pointing along \hat{z} and coupled to orbital degrees of freedom with an effective strength given by

$$b(\mathbf{x}) = \frac{\phi_0}{2\pi} \Omega(\mathbf{x}), \quad (33)$$

where $\phi_0 = \frac{2\pi\hbar c}{e}$ is the flux quantum. This relationship arises from interpreting Eq. (31) as a magnetic field associated with a skyrmion texture. Namely, a skyrmion texture with topological charge

$$N = \int d^2x \frac{1}{4\pi} \epsilon_{\mu\nu} \mathbf{s} \cdot (\partial_\mu \mathbf{s} \times \partial_\nu \mathbf{s}), \quad (34)$$

translates into N flux quanta of an effective magnetic field seen by an electron.

This observation has direct implications for the coupling strength of the chiral interaction given in Eqs. (2) and (3). The appreciable strength of this coupling implies that skyrmion textures are capable of inducing strong orbital current effects. One such effect is the anomalous Hall response. The estimates provided above indicate that the anomalous Hall effect generated by spin texture is equivalent to the Hall effect induced by a large magnetic field. This behavior resembles the behavior observed in $\text{Nd}_2\text{Mo}_2\text{O}_7$ [59], where a non-coplanar spin texture led to a significant anomalous Hall effect.

We are interested in the instability of a spatially uniform magnetic order towards a twisted state with a nonzero gauge field \mathbf{a} . We therefore consider power-series expansion of the electronic energy in Eq. (29) in small \mathbf{a} . We neglect the longitudinal fluctuations of \mathbf{h} , which are gapped, focusing on the soft angular fluctuations, $\delta\mathbf{h}(\mathbf{x}) \perp \mathbf{h}$. For a slowly varying unit-vector field $\mathbf{s}(\mathbf{x}) = \mathbf{h}/|\mathbf{h}|$, the dependence on \mathbf{a} in the first term of Eq. (29), hereafter referred to as F_1 , is of the form given by the Peierls substitution $\mathbf{p} \rightarrow \mathbf{p} + \mathbf{a}\sigma_3$. The expansion in powers of \mathbf{a} , because of the gauge covariance of the free energy F_1 , must involve gauge-invariant quantities expressed as gradients of \mathbf{a} such as $b = \frac{\hbar c}{e} \hat{z} \cdot [\nabla \times \mathbf{a}]$. At first order in \mathbf{a} , the dependence on \mathbf{a} can be linked to orbital magnetization by following a standard argument from electromagnetic theory. Namely, for both the majority-spin and minority-spin carriers,

one can write the coupling between orbital currents and geometric vector potential as $\delta H = -\frac{1}{c}\mathbf{j} \cdot \mathbf{a}$, and then rewrite it in terms of the geometric magnetic field given in Eq. (33) as $-Mb$ using $\nabla \times M\hat{z} = \frac{1}{c}\mathbf{j}$ and $\frac{\hbar c}{e}\hat{z} \cdot [\nabla \times \mathbf{a}] = b$. In a similar manner, we can write terms second order in \mathbf{a}^2 as $\frac{1}{2}\chi b^2$, where χ is the orbital diamagnetic susceptibility. Putting everything together we arrive at

$$F_1 = \sum_{\pm} E_{\pm} - \Delta Mb + \frac{1}{2}\chi b^2, \quad \Delta M = M_+ - M_-,$$

$$E_{\pm} = \sum_k (\epsilon_k^{\pm} - \mu) f(\epsilon_k^{\pm}), \quad \chi = \chi_+ + \chi_-, \quad (35)$$

where the quantities M_{\pm} and χ_{\pm} are the orbital magnetizations and the Landau diamagnetic susceptibilities of the majority and minority spins, which develop in the presence of Stoner band splitting but in the absence of the pseudomagnetic field $b(\mathbf{x}) = \frac{\hbar c}{e}\hat{z} \cdot [\nabla \times \mathbf{a}]$ [see Eq. (33)].

Namely, we assume that the spin imbalance, established by exchange interactions, is a leading-order effect, whereas the geometric field $b(\mathbf{x})$ is a relatively small effect. This is so because an expansion in gradients of \mathbf{a} , carried out in the long-wavelength limit, can only generate a small correction to the energy, as expected from Goldstone theorem. Accordingly, the E_{\pm} contributions are the energies of spin-majority and spin-minority fermions in the bands with an exchange spin splitting, $\epsilon_k^s = \epsilon_k \mp h$, evaluated at $\mathbf{a} = 0$, whereas the second and third terms represent the dependence on the pseudomagnetic field $\nabla \times \mathbf{a}$, which vanishes for a spatially uniform \mathbf{a} . The diamagnetic susceptibility χ of BBG as a function of band occupancy was analyzed in Ref. [66].

The contributions $\mp M_{\pm}b$ describe orbital magnetization of spin-majority and spin-minority carriers, arising due to Berry curvature, coupled to the pseudomagnetic field. Crucially, both the conduction and valence bands contribute to M . Therefore, perhaps counterintuitively, both up-spin and down-spin contributions to M matter even if the conduction band is fully polarized. The values M_{\pm} depend on the band filling and will be discussed below. The sign \mp accounts for the fact that the Berry phase for the carriers with opposite spins, moving in a slowly varying texture $\mathbf{h}(\mathbf{x})$, has opposite signs, described by the σ_3 factor in Eq. (29). In this form, Eq. (29) describes the limit of a weak, nonquantizing pseudomagnetic field b , which is sufficient for the purpose of analyzing the transition from zero to nonzero b .

VI. STONER INSTABILITY IN THE ABSENCE OF THE CHIRAL EFFECT

Putting everything together, and for now ignoring the chiral interaction, we can write the system energy in the absence of pseudomagnetic field b as

$$F = \int d^2x \left[E_+ + E_- + \frac{\hbar^2}{2U(0)} + \frac{J}{2}(\partial_{\mu}s)^2 \right]. \quad (36)$$

Using this expression, we can seek the ground state by comparing the energies of the ordered and disorder states. To account for the effect of a long-range $1/r$ density-density interaction without incorporating it explicitly in the mean-field analysis, we consider different states at the same total carrier density n . This approach is valid due to the large charging energy values $E_c = \frac{1}{2}V_0n^2$, which typically exceed other

energy scales in the system. When E_c is included in the analysis, the dependence of the total energy on n is dominated by the following terms:

$$\frac{V_0n^2}{2} - \mu n = \frac{V_0}{2} \left(n - \frac{\mu}{V_0} \right)^2 - \frac{\mu^2}{2V_0}. \quad (37)$$

These terms pin the density to $n = \frac{\mu}{V_0}$ regardless of the order type. Therefore, comparing energies of different states at the same μ in the presence of E_c is equivalent to comparing their energies at the same n .

To analyze the ordering described by Eq. (36) we proceed in two steps: First analyze the Stoner instability while temporarily ignoring b . Next, we consider the dependence on B and the transition from a uniform magnetic order to a twisting order.

In the absence of b , Eq. (36) describes the standard Stoner instability—a transition from a disordered state to a uniformly polarized state. Since the density of states in the quadratic Dirac band monotonically decreases as a function of energy, the ground state configuration is either fully spin polarized or spin unpolarized, depending on the band parameters and interaction strength. [For a more general band dispersion, partial spin polarization can also occur.] The energy density of a fully polarized phase with $n_+ = n$ and $n_- = 0$ is given by

$$F_{\text{fp}} = E_{\text{tot}}(n) - \frac{U_0n^2}{2} \quad (38)$$

where n is a given total carrier density. We have used Eq. (13). Here

$$E_{\text{tot}}(n) = \int_0^{\sqrt{4\pi n}} \frac{d^2k}{4\pi^2} \epsilon_k \quad (39)$$

represents the total kinetic energy of electrons of density n in one spin one valley in the absence of interaction. Similarly, the energy of unpolarized state where $n_+ = n_- = n/2$ is given by

$$F_{\text{unp}} = 2E_{\text{tot}}(n/2). \quad (40)$$

Here, we have used $h = 0$ in unpolarized phase. For our quadratic Dirac band, E_{tot} takes the following form:

$$E_{\text{tot}}(n) = \frac{mD^2}{4\pi} (\log(x + \sqrt{1+x^2}) + x\sqrt{1+x^2}), \quad (41)$$

where $x = \frac{2\pi n}{mD}$ is a dimensionless density parameter. The regime of interest is that of strong exchange interaction, which corresponds to low values $n \ll 2mD$. In this case, we can use power-series expansion $E_{\text{tot}}(n) = \frac{mD^2}{2\pi} (x + \frac{5}{12}x^3 + \dots)$. This allows a direct comparison of the energies of polarized and unpolarized states. Simple algebra then predicts the fully polarized state to win when

$$\frac{n}{D} < \frac{2m^2U_0}{5\pi^2}. \quad (42)$$

Therefore, the phase boundary is a straight line on the D - n phase diagram (see Fig. 1). This phase transition is first-order since the full polarization occurs abruptly.

VII. THE CHIRAL EFFECT AND ENERGETICS OF SPIN TEXTURES

Next, we consider spin textures $s(\mathbf{x})$ and derive the condition for skyrmion proliferation in the presence of chiral

interaction. From Eqs. (35) and (36), we see that system energy depends on s as $E_s = \int d^2x [\frac{1}{2}(\partial_\mu S_\alpha)^2 \mp \Delta M b + \frac{\chi}{2} b^2]$. Therefore, the spin texture enters the energetics in two ways: through pseudomagnetic field b , which is proportional to the spin-chirality density Eq. (31), and through the spin-stiffness energy $\frac{1}{2}J(\partial_\mu s)^2$. However, the latter contribution has a lower bound associated with spin chirality

$$\frac{1}{2} \int d^2x (\partial_\mu s)^2 \geq \frac{1}{2} \int d^2x |\epsilon_{\mu\nu} s \cdot (\partial_\mu s \times \partial_\nu s)|.$$

This relation follows from the well-known identity [26],

$$\int d^2x [(\partial_\mu s)^2 \mp \epsilon_{\mu\nu} s \cdot (\partial_\mu s \times \partial_\nu s)] \quad (43)$$

$$= \frac{1}{2} \int d^2x (\partial_\mu s \pm \epsilon_{\mu\nu} s \times \partial_\nu s)^2 \geq 0. \quad (44)$$

Expressing the stiffness energy through $|b|$ gives

$$E_s[b] = \int d^2x \left[-\Delta M b + \frac{2Je}{\hbar c} |b| + \frac{\chi}{2} b^2 \right]. \quad (45)$$

Naturally, the quantity $E_s[b]$ is only well-defined when spin polarization occurs, with b nonzero for a chiral spin texture and zero for a uniformly polarized state. We can now derive the condition for spin textures to be favored. The free energy in Eq. (45) gives the threshold for nucleating chiral spin textures in the ground state,

$$\Delta M \geq 2Je/\hbar c. \quad (46)$$

As a reminder, $\Delta M = M_+ - M_-$, $M_\pm = M(\mu \pm h)$ in one particular valley. Below, without loss of generality, we focus on K valley.

The net orbital magnetization of all electrons in one valley is governed by the Dirac band and its Berry curvature. This quantity, evaluated in our particle-hole-symmetric Dirac model, takes a simple form (see Ref. [60] and Appendix),

$$M_K(\mu) = \begin{cases} \frac{eD}{2\pi\hbar c}, & \mu > D \\ \frac{e\mu}{2\pi\hbar c}, & -D < \mu < D \\ -\frac{eD}{2\pi\hbar c}, & \mu < -D \end{cases}, \quad (47)$$

taking opposite values in valleys K and K' . This result is derived following the approach in Ref. [60], where a similar result was established for a monolayer graphene with a staggered sublattice potential. Reference [60] derived the valley-dependent magnetization in a gapped Dirac band, arriving at a relation between the orbital magnetization (per spin) and the band Berry curvature $\Omega(k)$,

$$M = \frac{e}{\hbar} \int \frac{d^2k}{(2\pi)^2} \mu \Omega(k) f(\epsilon_k) \quad (48)$$

where $\Omega(k)$ is of opposite signs in the particle and hole bands, $f(\epsilon_k)$ is the Fermi-Dirac distribution. However, as argued in Ref. [60], this relation between M and $\Omega(k)$ holds for a generic band with particle-hole symmetry.

Applying this formalism to quadratic Dirac band model yields the orbital magnetization in Eq. (47). We note that the dependence in Eq. (47), with M being constant in each band, is a unique property of the quadratic Dirac band dispersion, Eq. (6). A more general band dispersion would yield M that depends on doping in each band. These points are further discussed in Appendix, where, for illustration, the orbital

magnetization given in Eq. (47) is derived without invoking the Berry phase.

For a fully spin-polarized state at a carrier density n , $M_+ = \frac{eD}{2\pi\hbar c}$ whereas M_- depends on density. To calculate M_- we first calculate the chemical potential using $\mu + h = \sqrt{D^2 + (\frac{4\pi n}{2m})^2}$, which gives

$$\mu = \sqrt{D^2 + (2\pi n/m)^2} - U(0) \frac{n}{2} \sim D - U(0) \frac{n}{2}, \quad (49)$$

where the terms $O(n^2)$ were ignored since we are interested in the low-density regime. Plugging this into Eq. (47) yields

$$M_- = M(\mu - h) = (D - U(0)n) \frac{e}{2\pi\hbar c}. \quad (50)$$

As a result, the quantity $\Delta M = M_+ - M_-$ equals

$$\Delta M = U(0)n \frac{e}{2\pi\hbar c}. \quad (51)$$

Plugging this into Eq. (46) and using an estimate for spin stiffness obtained above, $J \sim \frac{\xi^2 \hbar^2}{U(0)}$, we find a condition for the transition from a fully polarized state to a chiral spin state,

$$\frac{eU(0)n}{2\pi\hbar c} \geq \frac{2e}{\hbar c} \frac{\xi^2 U(0)n^2}{4}. \quad (52)$$

This condition can be expressed in terms of carrier density and the correlation length ξ introduced in Sec. II,

$$n\xi^2 \leq \frac{1}{\pi}. \quad (53)$$

Since our mean-field analysis works for ξ exceeding the Fermi wavelength λ_F , the condition in Eq. (53) is marginally met. The threshold Eq. (53) can be further softened in multilayer graphene (such as trilayer, quadlayer, or pentalayer) since ΔM is proportional to the valley Chern number. For N -layer graphene, in a simplest model, C can take values that scale with the number of layers, $C = N/2$. As a result, the threshold softens to

$$n\xi^2 \leq \frac{C}{\pi}. \quad (54)$$

Using these results, we can predict schematic phase diagram in which the chiral phase (skyrmions) coexists with a uniformly spin-polarized phase, as shown in Fig. 1.

Applying the condition for instability given in Eq. (54) toward skyrmion texture to realistic systems requires estimating the values of ξ obtained from microscopic parameters. In system of interest, the carrier density n_c at the onset of Stoner transition can be estimated from Eq. (42). For interaction strength $U(0) = 5 \times 10^3$ meV nm², a band mass $m = 0.03m_e$ and a typical high value [13–17] $D = 100$ meV, it predicts Stoner instability at $n_c \sim 3 \times 10^{11}$ cm⁻². This carrier density indeed lies within the density range where the Stoner instability is observed [13–17]. Equation (53) then predicts that to nucleate skyrmions the characteristic lengthscale ξ must satisfy $\xi \lesssim 15$ nm, a value comparable to the screening length of Coulomb interaction in realistic settings. To further stabilize the chiral spin texture, one can reduce the spin stiffness J , which can be achieved by suppressing the correlation length of the spin-spin exchange interaction.

A phase diagram describing the competition between the orders described above is shown in Fig. 1. The transition line from uniformly polarized phase to skyrmion phase is given

by Eq. (53). We note that, compared to the transition line between the uniformly polarized phase and unpolarized phase, the transition line between skyrmion phase and unpolarized phase is pushed slightly into the unpolarized phase. This is because when skyrmion condenses, the energy contribution from pseudomagnetic field Eq. (45) is always negative and tends to stabilize ordered state. This phase boundary is a first-order phase transition because the translation symmetry and the spin SU(2) symmetry are simultaneously broken on this line.

We emphasize that our analysis above focused on the case of fully spin-polarized phase. Extending it to partially spin-polarized phases, where both spin-up and spin-down Fermi seas exist, encounters a subtle issue. Namely, for a partially spin-polarized quadratic Dirac band, the quantity ΔM naively vanishes because of the orbital magnetization being constant for μ values within the conduction and hole bands [see Eq. (47)]. It is interesting to note that ΔM also vanishes for the linear Dirac band, cubic Dirac band, and so on. However, this is almost certainly merely a coincidence, i.e., a result specific for ideal Dirac bands, which does not hold for realistic multilayer graphene bands. Indeed, for a generic graphene system, a chiral interaction is allowed by symmetry and is therefore expected to be nonzero on general grounds unless it vanishes accidentally.

We also note that the condition for skyrmion instability Eq. (53) can be softened in Dirac bands with larger valley Chern numbers, since ΔM is proportional to the total Hall conductivity in the lower band. Large valley Chern numbers can be achieved in graphene multilayers, such as trilayer, quadlayer, or pentalayer. Another appealing system is moiré graphene, where valley-Chern minibands [39] give rise to a doping-dependent orbital magnetization, potentially leading to a skyrmion instability triggered by spin-polarization onset.

The emergence of skyrmions through the mechanism discussed above can lead to different ground states depending on the interactions between skyrmions and the strength of the spin-order parameter zero-point or thermal fluctuations. Strong repulsive interactions would stabilize a chiral skyrmion crystal state, whereas strong fluctuations would lead to a chiral skyrmion liquid. Overall, these phases are expected to have properties similar to those of the vortex lattice and vortex liquid phases in superconductors [61–64]. Which of the two states—skyrmion crystal or skyrmion liquid—wins in the true ground state is an interesting topic for future work.

These two phases can be readily distinguished by transport measurements. In the presence of a valley polarization, such as the one seen in Bernal bilayer graphene as well as rhombohedral multilayer graphene systems and moiré graphene systems, we expect quantized topological Hall effect (QHE) in both states in the absence of an applied magnetic field [58,65]. This QHE contribution will appear in addition to (nonquantized) valley Hall effect.

So far we discussed skyrmions in one valley. If, however, the system is valley unpolarized but each valley exhibits Stoner spin-polarized order, skyrmions can occur in both valleys. The valleys K and K' are related by time-reversal symmetry, which requires opposite signs of the band Berry curvature and associated orbital magnetization, $M_K = -M_{K'}$. This imposes a peculiar relation between skyrmion chiralities in the two valleys, which can be understood from the chiral

interaction in Eq. (2),

$$\delta F = \int d^2x [-\Delta M_K b_K - \Delta M_{K'} b_{K'}], \quad (55)$$

where $\Delta M_K = M_{K,+} - M_{K,-}$ and $\Delta M_{K'} = M_{K',+} - M_{K',-}$, with the plus and minus indicating contributions of majority-spin and minority-spin carriers. Ignoring, at first, the intervalley exchange interaction, the system can be viewed as two identical Stoner problems with Berry curvatures of opposite signs in the two valleys. In this case, spin polarization directions in the two valleys are completely decoupled. Then, time-reversal symmetry of the Hamiltonian predicts equal degrees of spin polarization in valleys K and K' , and requires $M_{K,+} = -M_{K',+}$ and $M_{K,-} = -M_{K',-}$, namely, $\Delta M_+ = -\Delta M_-$. Indeed, under time reversal the majority (minority) spins in valley K are always mapped to the majority (minority) spins in valley K' . As a result, the $SU(2)_K \otimes SU(2)_{K'}$ symmetry of the microscopic Hamiltonian in the absence of intervalley exchange interactions, enforces the property $\Delta M_+ = -\Delta M_-$ regardless of whether spin polarization directions in the two valleys are parallel, antiparallel, or canted relative to one another. Therefore, in this case, the system will favor spin textures of opposite chiralities in the two valleys.

In realistic systems, however, the spins in the two valleys are weakly coupled by intervalley exchange interactions, which are much weaker than the intravalley interactions. The intervalley exchange is expected to be of a ferromagnetic sign in the regime of low carrier density [68]. To optimize this intervalley interaction, spin textures in valleys K and K' would need to be of identical direction and sign, i.e. $s_K(\mathbf{x}) = s_{K'}(\mathbf{r})$. However, this would result in equal-sign chirality densities in valleys K and K' . Such spin textures do not optimize the chiral interaction in Eq. (55), which favors opposite chiral densities in valleys K and K' . Therefore, in this case, our system is expected to exhibit a frustration effect—the energies of all terms in the Hamiltonian cannot be simultaneously optimized. As a result, many states can be envisaged as candidates for the ground state. One possibility is a two-valley chiral liquid where spin long-range order is washed out, but the chirality densities being of opposite signs in two valleys and exhibiting a long-range order. Another interesting option is a staggered skyrmion lattice, in which skyrmions formed by electrons in valleys K and K' are arranged in two interpenetrating lattices. Understanding such frustrated skyrmion phases represents an interesting direction for future work.

When time reversal is not spontaneously broken (no valley polarization), one expects a quantized topological valley Hall effect but no charge Hall effect, since the time-reversal symmetry requires skyrmions in valleys K and K' to have opposite chiralities. In addition, the longitudinal transport will be very different in the two phases—vanishing for skyrmion crystal and nonzero for skyrmion liquid, dual to that of superconducting vortex crystals and liquids.

VIII. SOME IMPLICATIONS OF THE CHIRAL EFFECT

In conclusion, this paper predicts a geometric spin-orbit coupling that arises in spin-polarized bands endowed with Berry curvature. The mechanism underpinning this coupling is that a spin of an electron moving through a spin texture is rotated in spin space. This spin-rotation effect, arising due to

an electron spin being locked to the local spin-quantization axis and tracking it along the electron trajectory, is described by a spin-dependent geometric phase. The adiabatic regime in which the geometric phase picture applies occurs when the Stoner spin gap is large compared to $\hbar v/\ell$, where ℓ is the characteristic spatial lengthscale of the spin-texture modulation and v is Fermi velocity.

This coupling leads to an instability of a uniformly spin-polarized state towards skyrmions. Occurring in an itinerant magnetic system, the skyrmions have several interesting properties. One is that they act on electrons as a geometric pseudomagnetic field, such that each skyrmion effectively generates one flux quantum of the field. The effective strength of this field is proportional to skyrmion density n_s and can be expressed as

$$b_{\text{eff}} = 4.13 \times 10^{-11} \times n_s [\text{cm}^{-2}] \text{ Tesla}. \quad (56)$$

For skyrmion density of $n_s \approx 10^{10} \text{ cm}^{-2}$ this predicts b_{eff} on the order 0.5 Tesla. The field B_{eff} grows rapidly as n_s increases. The Landau levels induced by b_{eff} introduce a new energy scale, which governs the skyrmion-induced topological gap in the system spectrum.

The geometric field b_{eff} , if present, would result in a topological Hall effect, manifested through a nonvanishing Hall conductivity occurring in the absence of an applied magnetic field. Because the geometric magnetic field has opposite signs for carriers with opposite spins, this Hall conductivity will exhibit a characteristic dependence on spin polarization, distinguishing it from the typical charge Hall conductivity. At carrier densities corresponding to ν electrons per skyrmion, where ν is an integer, the system will host ν fully filled skyrmion-induced Landau levels, leading to a quantized Hall conductivity

$$\sigma_{\text{H}} = \nu \frac{e^2}{h}. \quad (57)$$

For skyrmion crystal or liquid of a high density such that the number of electrons per skyrmion is small, this scenario predicts a state with large B_{eff} and a large topological gap.

In the extreme limit, when the skyrmion density achieved through this mechanism is large enough to be close to the density of itinerant carriers, the system can spontaneously adopt an insulating ground state where all electrons occupy one or several lowest Landau levels. This scenario may potentially apply to the quantized Hall phases recently observed in pentalayer graphene in the absence of a magnetic field [67,69]. The predicted phase diagram (Fig. 1), in which the chiral spin texture emerges at low carrier density, aligns with the density regime where the quantized Hall effect is observed in pentalayer graphene. The predicted dependence on the number of layers, implying that more layers tend to lower the threshold for the onset of spin chirality, potentially explains why this effect occurs in pentalayer rather than bilayer and trilayer systems.

ACKNOWLEDGMENTS

This work greatly benefited from discussions with Eli Zeldov, Steven Kivelson, and Patrick Lee. We acknowledge support from the Science and Technology Center for Integrated Quantum Materials, National Science Foundation Grant No. DMR1231319.

APPENDIX: VALLEY-DEPENDENT ORBITAL MAGNETIZATION IN GRAPHENE BILAYER

To gain more insight into the physics of the orbital magnetization, Eq. (47), here we rederive this known result [60] by a method that does not explicitly use Berry curvature. Our plan is to calculate the orbital magnetization in an individual graphene valley using thermodynamic relation

$$M_K = -\frac{\partial \Xi_K}{\partial B}, \quad (A1)$$

where Ξ_K is the thermodynamic potential of electrons in this valley, defined as

$$\Xi_K = \sum_{\alpha} (\epsilon_{\alpha} - \mu) f(\epsilon_{\alpha}), \quad f(\epsilon) = \frac{1}{e^{\beta(\epsilon - \mu)} + 1}, \quad (A2)$$

where ϵ_{α} are the Landau level energies in the particle and hole bands, labeled by $\alpha = \{\pm, n\}$.

In order to obtain the magnetization at $B = 0$ we first calculate the Landau level energies ϵ_{α} and, by using the Euler-Maclaurin summation formula, extract the part of the sum over α in Eq. (A2), which is linear in B at small B . As we will see, the contribution linear in B is equal to that originating from the anomalous Landau levels reduced by a factor of two, as discussed below. We will end this section by discussing the general character of this result and its relation to the spectral flow.

The Landau level energies can be derived directly from the BBG Hamiltonian [18,70]. For illustration, here we do it for a simplified form of the Hamiltonian involving no trigonal warping terms

$$H_K(p) = \begin{pmatrix} D + \frac{p^2}{2m_0} + \frac{p^2}{2m_a} & -\frac{(p_1 - ip_2)^2}{2m} \\ -\frac{(p_1 + ip_2)^2}{2m} & -D - \frac{p^2}{2m_0} + \frac{p^2}{2m_a} \end{pmatrix}. \quad (A3)$$

Magnetic field can be incorporated in the Hamiltonian through the substitution $\mathbf{p} \rightarrow \mathbf{p} - \frac{e}{c} \mathbf{a}$. We will first carry out the analysis ignoring the terms $p^2/2m_0$ and $p^2/2m_a$. This is justified because these two terms are subleading for a realistic BBG band [18]. For the same reason we ignore the trigonal warping term [not shown in Eq. (A3)]. To illustrate the generality of our results, we will subsequently present the analysis for the full Hamiltonian in Eq. (A3), finding that the quadratic terms $p^2/2m_0$ and $p^2/2m_a$ do not affect the result.

Next we consider the Landau levels formed in the presence of a B field, at first excluding the quadratic terms in the diagonal elements. As is well known, in each valley— K or K' —the Hamiltonian in Eq. (A3), with the quadratic terms excluded, in the presence of a magnetic field generates three groups of Landau levels: (i) a pair of anomalous Landau levels at the edges of the hole band for valley K and particle band for valley K' , and (ii) two sequences of Landau levels in the particle and hole bands that are related by particle-hole symmetry. The energies of these Landau levels in valley K can be written as [66]

$$\begin{aligned} \epsilon_{\pm, n} &= \epsilon_{\pm}(x_n) = \pm \sqrt{x_n^2 - \frac{1}{4} \hbar^2 \omega_c^2 + D^2}, \quad n \geq 2, \\ \epsilon_{0,1} &= -D, \quad x_n = \hbar \omega_c \left(n - \frac{1}{2} \right), \end{aligned} \quad (A4)$$

where $\omega_c = eB/mc$ is the cyclotron frequency. For valley K' similar expressions arise; however, the anomalous Landau levels are positioned at the particle band edge, $\epsilon_{0,1} = D$.

Accordingly, the thermodynamic potential Ξ_K in the presence of a B field is a sum of three contributions

$$\Xi_K = \Xi_+ + \Xi_- + \Xi_{01}, \quad (\text{A5})$$

where

$$\Xi_{\pm} = \frac{eB}{hc} \sum_n (\epsilon_{\pm,n} - \mu) f(\epsilon_{\pm,n}), \quad (\text{A6})$$

$$\Xi_{01} = \frac{2eB}{hc} (-D - \mu) f(-D), \quad (\text{A7})$$

with eB/hc representing the numbers of electrons in each Landau level per unit area.

Magnetization is given by the linear [$O(B)$] term in $\Xi_K(B)$. The $O(B)$ contribution from the anomalous levels in each valley is already clearly written in Eq. (A7). To calculate the $O(B)$ contribution from Ξ_{\pm} we use the Euler-Maclaurin formula, which approximates a sum by an integral. For the contribution of the particle band we have

$$\begin{aligned} \Xi_+ = \frac{eB}{hc} \left[\frac{1}{\hbar\omega_c} \int_{x_{n=2}}^{\infty} dx (\epsilon(x) - \mu) f(\epsilon(x)) \right. \\ \left. + \frac{1}{2} (\epsilon(x_{n=2}) - \mu) f(\epsilon(x_{n=2})) \right] + O(B^2), \quad (\text{A8}) \end{aligned}$$

where $x_{n=2} = \frac{3}{2}\hbar\omega_c$, see Eq. (A4). Here we have used $\epsilon(\infty)f(\infty) = 0$. Working out the integral gives

$$\Xi_+ = -\frac{eB}{hc} (D - \mu) f(D) + O(B^2). \quad (\text{A9})$$

Similarly, the $O(B)$ contribution of the lower-band Landau levels is given by

$$\Xi_- = -\frac{eB}{hc} (-D - \mu) f(-D) + O(B^2). \quad (\text{A10})$$

After plugging Eqs. (A7), (A9), and (A10) into Eqs. (A1) and (A5), we arrive at

$$M_K(\mu) = \begin{cases} \frac{2eD}{2\pi\hbar c}, & \mu > D \\ \frac{e(\mu+D)}{2\pi\hbar c}, & -D < \mu < D \\ 0, & \mu < -D \end{cases} \quad (\text{A11})$$

We note that this dependence differs by a constant shift of $\Delta M_K = \frac{eD}{2\pi\hbar c}$ from the result in Eq. (47) that was inferred from the general expression for orbital magnetization obtained in Ref. [60]. This constant shift arises from the way the contribution of the deep-lying levels is cut off, which is different from the conventional way [60]. However, this difference is

immaterial because the deep-lying states, due to their uncertain valley character and identical occupancies for opposite spins, are not expected to affect physical observables.

Indeed, at the bottom of the graphene band the carrier states cannot be unambiguously identified with the K and K' valleys. Therefore the ambiguity arising from the cutoff is a matter of convention rather than a physical effect. Furthermore, the quantity that matters for the physics of interest is the difference of the contributions from the spin-up and spin-down bands, $\Delta M = M_{K,\uparrow} - M_{K,\downarrow}$. The bands for opposite spins are filled equally at the bottom, such that the contributions of the deep-lying states to $M_{K,\uparrow}$ and $M_{K,\downarrow}$ cancel each other.

The meaning of the resulting dependence $M_K(\mu)$, in which M_K is constant when the Fermi level lies within one of the bands, can be understood in terms of a spectral flow induced by a variation of B . Namely, the role of the Landau levels moving up and down is merely to cancel half of the contribution to magnetization M_K of the anomalous Landau levels in the corresponding bands. As a result, there is no μ dependence when the Fermi level lies outside the gap. In that each anomalous level contributes a half of the ‘nominal value’ of a single Landau level. This contribution comes with a plus sign or a minus sign depending on whether an anomalous Landau level is present or absent for the band and valley in question. The resulting dependence of orbital magnetization is identical for the K and K' valleys up to a sign reversal, $M_K(\mu) = -M_{K'}(\mu)$.

This analysis can be applied to a realistic model of Bernal bilayer graphene, where the band Hamiltonian takes a more complicated form [18]. Here we show that adding the two quadratic terms given in Eq. (A3) that were neglected temporarily, does not alter the result for $M_K(\mu)$.

The term $p^2/2m_a$ is an identity matrix in the sublattice variables. As a result, it merely shifts the energy eigenvalues without affecting the electron wavefunction that determines the orbital magnetization. Therefore, this term only affect the diamagnetic susceptibility but does not affect the magnetization at $B = 0$. Indeed, adding it in Eq. (A8) yields an $O(B^2)$ contribution to the thermodynamic potential, changing somewhat the diamagnetic susceptibility but not changing $M_K(\mu)$.

The term $p^2/2m_0$ has a σ_3 sublattice structure. Such a term does affect the wavefunctions, and yet, this term alone does not break the particle-hole symmetry. Also, this term does not affect the energy of the lowest Landau level in the particle band. As a result, the two conditions necessary for the reasoning above [from Eqs. (A5)–(A10)]—the particle-hole symmetry and the presence of two anomalous Landau levels—remain valid. As a result, the answer for magnetization given above remains unchanged.

- [1] J. M. B. Lopes dos Santos, N. M. R. Peres, and A. H. Castro Neto, Graphene bilayer with a twist: Electronic structure, *Phys. Rev. Lett.* **99**, 256802 (2007).
- [2] E. J. Mele, Commensuration and interlayer coherence in twisted bilayer graphene, *Phys. Rev. B* **81**, 161405(R) (2010).
- [3] E. Suárez Morell, J. D. Correa, P. Vargas, M. Pacheco, and Z. Barticevic, Flat bands in slightly twisted bilayer graphene: Tight-binding calculations, *Phys. Rev. B* **82**, 121407(R) (2010).

- [4] R. Bistritzer and A. H. MacDonald, Moiré bands in twisted double-layer graphene, *Proc. Natl. Acad. Sci. USA* **108**, 12233 (2011).
- [5] F. Guinea and N. R. Walet, Electrostatic effects, band distortions, and superconductivity in twisted graphene bilayers, *Proc. Natl. Acad. Sci. USA* **115**, 13174 (2018).
- [6] E. Y. Andrei and A. H. MacDonald, Graphene bilayers with a twist, *Nat. Mater.* **19**, 1265 (2020).

- [7] Y. Cao, V. Fatemi, S. Fang, K. Watanabe, T. Taniguchi, E. Kaxiras, and P. Jarillo-Herrero, Unconventional superconductivity in magic-angle graphene superlattices, *Nature (London)* **556**, 43 (2018).
- [8] Y. Cao, V. Fatemi, A. Demir, S. Fang, S. L. Tomarken, J. Y. Luo, J. D. Sanchez-Yamagishi, K. Watanabe, T. Taniguchi, E. Kaxiras, and R. C. Ashoori, Correlated insulator behaviour at half-filling in magic-angle graphene superlattices, *Nature (London)* **556**, 80 (2018).
- [9] Y. Cao, D. Rodan-Legrain, O. Rubies-Bigorda, J. M. Park, K. Watanabe, T. Taniguchi, and P. Jarillo-Herrero, Tunable correlated states and spin-polarized phases in twisted bilayer-bilayer graphene, *Nature (London)* **583**, 215 (2020).
- [10] U. Zondiner, A. Rozen, D. Rodan-Legrain, Y. Cao, R. Queiroz, T. Taniguchi, K. Watanabe, Y. Oreg, F. von Oppen, A. Stern, and E. Berg, Cascade of phase transitions and Dirac revivals in magic-angle graphene, *Nature (London)* **582**, 203 (2020).
- [11] D. Wong, K. P. Nuckolls, M. Oh, B. Lian, Y. Xie, S. Jeon, K. Watanabe, T. Taniguchi, B. A. Bernevig, and A. Yazdani, Cascade of electronic transitions in magic-angle twisted bilayer graphene, *Nature (London)* **582**, 198 (2020).
- [12] Y. Saito, F. Yang, J. Ge, X. Liu, T. Taniguchi, K. Watanabe, J. I. A. Li, and E. Berg, and A. F. Young, Isospin Pomeranchuk effect in twisted bilayer graphene, *Nature (London)* **592**, 220 (2021).
- [13] A. M. Seiler, F. R. Geisenhof, F. Winterer, K. Watanabe, T. Taniguchi, T. Xu, F. Zhang, and R. T. Weitz, Quantum cascade of correlated phases in trigonally warped bilayer graphene, *Nature (London)* **608**, 298 (2022).
- [14] H. Zhou, L. Holleis, Y. Saito, L. Cohen, W. Huynh, C. L. Patterson, F. Yang, T. Taniguchi, K. Watanabe, and A. F. Young, Isospin magnetism and spin-polarized superconductivity in Bernal bilayer graphene, *Science* **375**, 774 (2022).
- [15] S. C. de la Barrera, S. Aronson, Z. Zheng, K. Watanabe, T. Taniguchi, Q. Ma, P. Jarillo-Herrero, and R. Ashoori, Cascade of isospin phase transitions in Bernal-stacked bilayer graphene at zero magnetic field, *Nat. Phys.* **18**, 771 (2022).
- [16] H. Zhou, T. Xie, T. Taniguchi, K. Watanabe, and A. F. Young, Superconductivity in rhombohedral trilayer graphene, *Nature (London)* **598**, 434 (2021).
- [17] H. Zhou, T. Xie, A. Ghazaryan, T. Holder, J. R. Ehrets, E. M. Spanton, T. Taniguchi, K. Watanabe, E. Berg, M. Serbyn, and A. F. Young, Half- and quarter-metals in rhombohedral trilayer graphene, *Nature (London)* **598**, 429 (2021).
- [18] E. McCann and M. Koshino, The electronic properties of bilayer graphene, *Rep. Prog. Phys.* **76**, 056503 (2013).
- [19] Z. Dong, O. Ogunnaike, and L. Levitov, Collective excitations in chiral Stoner magnets, *Phys. Rev. Lett.* **130**, 206701 (2023).
- [20] A. Fert, N. Reyren, V. Cros, Magnetic skyrmions: Advances in physics and potential applications, *Nat. Rev. Mater.* **2**, 17031 (2017).
- [21] N. Nagaosa and Y. Tokura, Topological properties and dynamics of magnetic skyrmions, *Nat. Nanotech.* **8**, 899 (2013).
- [22] A. N. Bogdanov and U. K. Rössler, Chiral symmetry breaking in magnetic thin films and multilayers, *Phys. Rev. Lett.* **87**, 037203 (2001).
- [23] M. Kataoka and O. Nakanishi, Helical spin density wave due to antisymmetric exchange interaction, *J. Phys. Soc. Jpn.* **50**, 3888 (1981).
- [24] B. Binz, A. Vishwanath, and V. Aji, Theory of the helical spin crystal: A candidate for the partially ordered state of MnSi, *Phys. Rev. Lett.* **96**, 207202 (2006).
- [25] O. Nakanishi, A. Yanase, A. Hasegawa, and M. Kataoka, The origin of the helical spin density wave in MnSi, *Solid State Commun.* **35**, 995 (1980).
- [26] A. M. Polyakov, *Gauge Fields and Strings* (Harwood Academic, New York, 1987).
- [27] U. K. Röbler, A. N. Bogdanov, and C. Pfleiderer, Spontaneous skyrmion ground states in magnetic metals, *Nature (London)* **442**, 797 (2006).
- [28] S. Mühlbauer, B. Binz, F. Jonietz, C. Pfleiderer, A. Rosch, A. Neubauer, R. Georgii, and P. Böni, Skyrmion lattice in a chiral magnet, *Science* **323**, 915 (2009).
- [29] A. Neubauer, C. Pfleiderer, B. Binz, A. Rosch, R. Ritz, P. G. Niklowitz, and P. Böni, Topological Hall effect in the A phase of MnSi, *Phys. Rev. Lett.* **102**, 186602 (2009).
- [30] X. Z. Yu, Y. Onose, N. Kanazawa, J. H. Park, J. H. Han, Y. Matsui, N. Nagaosa, and Y. Tokura, Real-space observation of a two-dimensional skyrmion crystal, *Nature (London)* **465**, 901 (2010).
- [31] S. Seki, X. Z. Yu, S. Ishiwata, and Y. Tokura, Observation of skyrmions in a multiferroic material, *Science* **336**, 198 (2012).
- [32] T. Schulz, R. Ritz, A. Bauer, M. Halder, M. Wagner, C. Franz, C. Pfleiderer, K. Everschor, M. Garst, and A. Rosch, Emergent electrodynamics of skyrmions in a chiral magnet, *Nat. Phys.* **8**, 301 (2012).
- [33] S. Heinze, K. Von Bergmann, M. Menzel, J. Brede, A. Kubetzka, R. Wiesendanger, G. Bihlmayer, and S. Blügel, Spontaneous atomic-scale magnetic skyrmion lattice in two dimensions, *Nat. Phys.* **7**, 713 (2011).
- [34] W. Jiang, G. Chen, K. Liu, J. Zang, S. G. Te Velthuis, and A. Hoffmann, Skyrmions in magnetic multilayers, *Phys. Rep.* **704**, 1 (2017).
- [35] A. C. Neto, F. Guinea, N. M. R. Peres, K. S. Novoselov, and A. K. Geim, The electronic properties of graphene, *Rev. Mod. Phys.* **81**, 109 (2009).
- [36] T. Okubo, S. Chung, and H. Kawamura, Multiple-q states and the skyrmion lattice of the triangular-lattice Heisenberg antiferromagnet under magnetic fields, *Phys. Rev. Lett.* **108**, 017206 (2012).
- [37] A. O. Leonov and M. Mostovoy, Multiply periodic states and isolated skyrmions in an anisotropic frustrated magnet, *Nat. Commun.* **6**, 8275 (2015).
- [38] S. Hayami, R. Ozawa, and Y. Motome, Effective bilinear-biquadratic model for noncoplanar ordering in itinerant magnets, *Phys. Rev. B* **95**, 224424 (2017).
- [39] J. C. Song, P. Samutpraphoot, and L. S. Levitov, Topological Bloch bands in graphene superlattices, *Proc. Natl. Acad. Sci. USA* **112**, 10879 (2015).
- [40] E. V. Castro, N. M. R. Peres, T. Stauber, and N. A. P. Silva, Low-density ferromagnetism in biased bilayer graphene, *Phys. Rev. Lett.* **100**, 186803 (2008).
- [41] T. Bömerich, L. Heinen, A. Rosch, Skyrmion and tetarton lattices in twisted bilayer graphene, *Phys. Rev. B* **102**, 100408 (2020).
- [42] E. Khalaf, S. Chatterjee, N. Bultinck, M. P. Zaletel, and A. Vishwanath, Charged skyrmions and topological origin of superconductivity in magic-angle graphene, *Sci. Adv.* **7**, eabf5299 (2021).

- [43] S. L. Sondhi, and A. Karlhede, and S. A. Kivelson, and E. H. Rezayi, Skyrmions and the crossover from the integer to fractional quantum Hall effect at small Zeeman energies, *Phys. Rev. B* **47**, 16419 (1993).
- [44] A. H. MacDonald, H. A. Fertig, and Luis Brey, Skyrmions without sigma models in quantum Hall ferromagnets, *Phys. Rev. Lett.* **76**, 2153 (1996).
- [45] H. A. Fertig, L. Brey, R. Côté, A. H. MacDonald, A. Karlhede, and S. L. Sondhi, Hartree-Fock theory of Skyrmions in quantum Hall ferromagnets, *Phys. Rev. B* **55**, 10671 (1997).
- [46] K. Nomura and A. H. MacDonald, Quantum Hall ferromagnetism in graphene, *Phys. Rev. Lett.* **96**, 256602 (2006).
- [47] K. Yang, S. Das Sarma, and A. H. MacDonald, Collective modes and skyrmion excitations in graphene SU(4) quantum Hall ferromagnets, *Phys. Rev. B* **74**, 075423 (2006).
- [48] H. Zhou, H. Polshyn, and T. Taniguchi *et al.*, Solids of quantum Hall skyrmions in graphene, *Nat. Phys.* **16**, 154 (2020).
- [49] X. Liu, G. Farahi, C. L. Chiu, Z. Papic, K. Watanabe, T. Taniguchi, M. P. Zaletel, and A. Yazdani, Visualizing broken symmetry and topological defects in a quantum Hall ferromagnet, *Science* **375**, 321 (2022).
- [50] P. Coleman, *Introduction to Many-Body Physics* (Cambridge University Press, Cambridge, 2015).
- [51] G. Baskaran and P. W. Anderson, Gauge theory of high-temperature superconductors and strongly correlated Fermi systems, *Phys. Rev. B* **37**, 580 (1988).
- [52] P. B. Wiegmann, Superconductivity in strongly correlated electronic systems and confinement versus deconfinement phenomenon, *Phys. Rev. Lett.* **60**, 821 (1988).
- [53] H. J. Schulz, Effective action for strongly correlated fermions from functional integrals, *Phys. Rev. Lett.* **65**, 2462 (1990).
- [54] L. B. Ioffe, V. Kalmeyer, and P. B. Wiegmann, Hall coefficient of the doped Mott insulator: A signature of parity violation, *Phys. Rev. B* **43**, 1219 (1991).
- [55] G. E. Volovik, Linear momentum in ferromagnets, *J. Phys. C: Solid State Phys.* **20**, L83 (1987).
- [56] K. Ohgushi, S. Murakami, and N. Nagaosa, Spin anisotropy and quantum Hall effect in the kagomé lattice: Chiral spin state based on a ferromagnet, *Phys. Rev. B* **62**, R6065 (2000).
- [57] T. Fujita, M. B. A. Jalil, S. G. Tan, and S. Murakami, Gauge fields in spintronics, *J. Appl. Phys.* **110**, 121301 (2011).
- [58] K. Hamamoto, M. Ezawa, and N. Nagaosa, Quantized topological Hall effect in skyrmion crystal, *Phys. Rev. B* **92**, 115417 (2015).
- [59] Y. Taguchi, Y. Oohara, H. Yoshizawa, N. Nagaosa, and Y. Tokura, Spin chirality, Berry phase, and anomalous Hall effect in a frustrated ferromagnet, *Science* **291**, 2573 (2001).
- [60] D. Xiao, W. Yao, and Q. Niu, Valley-contrasting physics in graphene: magnetic moment and topological transport, *Phys. Rev. Lett.* **99**, 236809 (2007).
- [61] B. A. Huberman and S. Doniach, Melting of two-dimensional vortex lattices, *Phys. Rev. Lett.* **43**, 950 (1979).
- [62] D. S. Fisher, M. P. Fisher, and D. A. Huse, Thermal fluctuations, quenched disorder, phase transitions, and transport in type-II superconductors, *Phys. Rev. B* **43**, 130 (1991).
- [63] J. Hu and A. H. MacDonald, Two-dimensional vortex lattice melting, *Phys. Rev. Lett.* **71**, 432 (1993).
- [64] G. Blatter, M. V. Feigel'man, V. B. Geshkenbein, A. I. Larkin, and V. M. Vinokur, Vortices in high-temperature superconductors, *Rev. Mod. Phys.* **66**, 1125 (1994).
- [65] B. Göbel, A. Mook, J. Henk, and I. Mertig, Unconventional topological Hall effect in skyrmion crystals caused by the topology of the lattice, *Phys. Rev. B* **95**, 094413 (2017).
- [66] M. Koshino and T. Ando, Anomalous orbital magnetism in Dirac-electron systems: Role of pseudospin paramagnetism, *Phys. Rev. B* **81**, 195431 (2010).
- [67] Z. Lu, T. Han, Y. Yao, A. P. Reddy, J. Yang, J. Seo, K. Watanabe, T. Taniguchi, L. Fu, and L. Ju, Fractional quantum anomalous Hall effect in multilayer graphene, *Nature (London)* **626**, 759 (2024).
- [68] Y. Z. You and A. Vishwanath, Kohn-Luttinger superconductivity and intervalley coherence in rhombohedral trilayer graphene, *Phys. Rev. B* **105**, 134524 (2022).
- [69] T. Han, Z. Lu, G. Scuri, J. Sung, J. Wang, T. Han, K. Watanabe, T. Taniguchi, H. Park, and L. Ju, Correlated insulator and Chern insulators in pentalayer rhombohedral-stacked graphene, *Nat. Nanotechnol.* **19**, 181 (2024).
- [70] E. McCann, and V. I. Fal'ko, Landau-level degeneracy and quantum Hall effect in a graphite bilayer, *Phys. Rev. Lett.* **96**, 086805 (2006).